

Two–Electron Effects in the Multiphoton Ionization of Magnesium with 400 nm 150 fs Pulses

D. Xenakis^{1,*}, N. E. Karapanagioti^{1,*} and D. Charalambidis^{1,2}

¹*Laser and Applications Division, Institute of Electronic Structure and Laser, Foundation for Research and Technology–Hellas, P.O.Box 1527, GR-711 10 Heraklion, Greece*

²*Physics Department, University of Crete, GR-713 10 Heraklion, Greece*

H. Bachau and E. Cormier

*Centre Lasers Intenses et Applications (Université Bordeaux I-CNRS), Université Bordeaux I,
351 Cours de la Libération, F-33405 Talence Cedex, France*

(August 22, 2021)

Abstract

The multiphoton ionization and photoelectron spectra of magnesium were studied at laser intensities of up to $6 \times 10^{13} \text{ Wcm}^{-2}$ using 150 fs laser pulses of a wavelength of 400 nm. The results indicated that a variety of different ionization mechanisms played a role in both types of spectra. A theoretical model describing the processes is presented and the routes to ionization are identified. The work demonstrates the significance of the two–electron nature of the atom in interpreting the experimental results.

PACS numbers: 32.80.Rm, 32.80.Fb, 32.80.Wr

Typeset using REVTeX

*Presently at: *Max–Planck–Institut für Quantenoptik, Hans–Kopfermannstrasse, D-85748 Garching, Germany*

I. INTRODUCTION

The behavior of atoms in intense electro-magnetic fields has been under investigation since the advent of the laser. Especially since the development of short-pulse, high-intensity systems, experiments have revealed a multitude of novel effects such as multiphoton ionization (MPI) [1], above threshold ionization (ATI) [2], harmonic generation [3,4] etc. Most of the theoretical models originally proposed to describe the observations involved essentially a single electron interacting with the electromagnetic field. This approximation has led to significant understanding of the atomic behavior in the field. However, the multi-electron nature of most atoms can play a significant role under certain circumstances. Theory then has to take into account multi-electron excitation, correlations between the electrons, multiple continua, i.e. the detailed atomic structure in order to be able to predict the atomic behavior. This fact emerges as both theoretical and experimental techniques become more advanced, enabling the exploration of new regimes and the detailed testing of theoretical models.

In multi-electron atoms, significant double excitation can take place leaving the ion not in the ionic ground state but in an excited state or possibly ejecting a second electron. In the alkaline earth atoms for example, the existence of doubly excited-state manifolds between the two ionic thresholds alters drastically the single-electron picture rendering it unsuitable. The conditions under which these effects may occur are easily within reach of present experimental setups. Past work by Dalwoo Kim et al [5], DiMauro et al [6] and van Druten et al [7] has looked into the multiphoton ionization of magnesium with nanosecond and picosecond laser pulse durations and indicated the importance of short pulse experiments in understanding the processes involved. At the same time, theoretical methods incorporating these effects are also being developed [8,9], creating the need for further experimental investigations.

In the present work we seek to investigate the extent to which electron correlations play a role in the high intensity regime for multi-electron atoms. We chose magnesium, a fairly low atomic weight alkaline earth element, as it is accessible to both experimental and theoretical investigation. We report measurements of the multiphoton single and double ionization and ATI of magnesium using 150 fs, 400 nm laser pulses. A theoretical model has been developed and applied which describes the processes leading to ionization and shows that the inclusion of one and two-electron effects are necessary for an accurate description. Measurements of the multiphoton ionization yield displayed the expected perturbative behavior for the production of the Mg^+ ion but showed unexpected features in the double ionization yield. The ATI electron spectra also exhibited complex structure, originating from a variety of single and double ionization mechanisms, whose relative importance changes as the intensity is varied. The theoretical treatment involved both a perturbation theory description including all correlation effects between the active electrons and additionally, for the ionization of Mg^+ , a non-perturbative approach.

II. METHOD

A. Experimental set-up

A plan of the experimental set-up is shown in figure 1. The laser employed consists of a titanium sapphire oscillator amplified in a regenerative amplifier utilizing a chirped pulse amplification technique [10]. The laser operates at 1 kHz repetition rate, with a measured pulse duration of ≈ 150 fs at a wavelength of ≈ 798 nm. The second harmonic of this beam was then produced using a focused geometry in a $250 \mu\text{m}$ thick BBO crystal. The harmonic radiation was separated from the co-propagating fundamental by employing three dichroic mirrors that were transparent to the fundamental (denoted by $M_{2\omega}$ in figure 1). The harmonic generation efficiency of this setup was $\approx 10\%$. The laser energy of the fundamental was set to be less than $300 \mu\text{J}$, thus producing a maximum of $\approx 30 \mu\text{J}$ of second harmonic radiation.

The resulting harmonic laser beam was focused in a time-of-flight spectrometer (TOF) by a MgF lens of 15 cm focal length. A half-wave plate was positioned prior to that in order to align the polarization of the light with the TOF tube axis. Under the conditions of the experiment, the lens did not affect significantly the beam either in terms of non-linear absorption or by pulse-front curvature at the focus [11]. The energy measurement was achieved with a fast vacuum photodiode which was cross-calibrated with an average power meter.

The time-of-flight spectrometer, which has a field-free flight tube of 15 cm oriented perpendicular to the laser propagation axis, is equipped with a μ -metal magnetic shield. This shield, in combination with a repeller plate and the appropriate polarity of the charged particle detector, allowed the use of the instrument alternately as an electron spectrometer and as an ion time-of-flight system. For the electron energy measurements the repeller was grounded, whereas for the operation of the TOF as a mass spectrometer the repeller was charged with a voltage of up to +1000 V. The charged particle detector at the end of the flight tube was a double micro-channel plate in a chevron configuration. Its front side was grounded for detecting electrons and at a negative voltage for ions.

An oven was inserted at the top of the interaction chamber filled with magnesium pellets which, when heated, produced an atomic beam as the vapor exited an aperture. The atomic beam met the laser beam and the time-of-flight tube at right angles.

The acquisition system was essentially the same for both electron and ion detection. The signal from the micro-channel plates first went through a fast amplifier and a discriminator. Subsequently, its time of arrival with respect to the laser pulse was recorded by a multiple-event time-digitizer card which was installed in a personal computer. The main feature of this card was that it could acquire and time one event per 0.5 ns time-bin with no dead-time between bins. Combined with the bandwidth of the cabling and electronic processing stages, the effective time resolution of the system was approximately one nanosecond. This acquisition system was not sensitive to the amplitude of the signal and hence it was operated in the event-counting regime. This meant that the number of events *in each bin* had to be less than one per laser pulse, a condition which was ensured throughout the measurement.

At the higher laser intensities, for which the counting method was no longer appropriate due to the increased ionization rates, the analogue signal was obtained directly from the micro-channel plates and recorded on a digital oscilloscope. For the ion yield versus laser intensity spectra, where data were recorded using both methods of acquisition, the data

were matched at several points in an intermediate regime. They were further cross-checked with data from the less abundant isotopes of magnesium which would be still in the counting regime at intensities for which the main peak was not. Lastly, to ensure that no space-charge effects were distorting the data, measurements were taken at different oven temperatures (and consequently atomic number densities) and compared. No rigorous absolute energy calibration of the electron spectrometer was performed. The calibration of the energy scale was based on the expected inter-peak separation of the several ATI peaks. This resulted in a determination of the relative peak positions to better than 0.1 eV, although the determination of the absolute peak positions was hindered by uncertainty in the zero time. Comparison to data with xenon was consistent with the magnesium results in so far as the energy calibration of the spectra was concerned, confirming the validity of the calibration. Xenon was also used to estimate the intensity of the laser at the interaction region [12–14] and compare it with the number obtained by estimating the focal spot size.

B. Theoretical modeling

We now propose a theory to describe the experimental results and explain most of the essential features. Magnesium in the present context is a rather complicated system since it involves many coupled states and different ionization channels. However, in that case, we were able to identify and isolate atomic states and transitions connected to the leading processes. These elements are summarized in figure 2. We consider that the electrons measured in the experiment are produced by 4 different processes. Two lead to the production of Mg^+ (single ionization to the ground state $\text{Mg}^+(3s)$ by absorption of 3 photons or to the first excited state $\text{Mg}^+(3p)$ by absorption of 4 photons) and are labeled process (1) and (2) respectively. Two other processes sequentially double ionize the system from the ion Mg^+ . Mg^{++} is thus produced by absorption of 4 photons from $\text{Mg}^+(3p)$ or by absorption of 5 photons from $\text{Mg}^+(3s)$. The basic assumption in the theoretical approach is that double ionization is produced through a sequential process. Therefore, double ionization through direct (coherent) absorption of 8 photons (see path (5) in figure 2) is neglected. Under these conditions, the population of each species is obtained by solving the following rate equations:

$$\begin{aligned}\dot{N}_{3s^2} &= -(\Gamma_{3s^2 \rightarrow 3sk_1}^{(3)} + \Gamma_{3s^2 \rightarrow 3pk_2}^{(4)}) N_{3s^2} \\ \dot{N}_{3s} &= \Gamma_{3s^2 \rightarrow 3sk_1}^{(3)} N_{3s^2} - \Gamma_{3sk_1 \rightarrow k_4k_1}^{(5)} N_{3s} \\ \dot{N}_{3p} &= \Gamma_{3s^2 \rightarrow 3pk_2}^{(4)} N_{3s^2} - \Gamma_{3pk_2 \rightarrow k_3k_2}^{(4)} N_{3p}\end{aligned}\tag{1}$$

with the initial conditions $N_{3s^2}(t = -\infty) = 1$ and all other populations set to zero. N_{3s^2} , N_{3s} and N_{3p} represent the time-dependent populations of $\text{Mg}(3s^2)$, $\text{Mg}^+(3s)$ and $\text{Mg}^+(3p)$ respectively. The time-dependent width $\Gamma_{3ln_1 \rightarrow n_2n_3}^{(p)}$ refers to the p -photon transition from the initial state $3ln_1$ to the final state n_2n_3 . When the specification of the angular momentum has been removed from the state notation (like in n_2n_3), the width includes the contribution from each accessible symmetry. k_n refers to the momentum of the electron ejected through the process labeled (n) in figure 2. The electron energies (reported in table I) are deduced from the energy conservation principle excluding laser induced level shifts. The atomic structure calculations providing the atomic energy levels and the transition cross-sections have been

described in detail in a precedent paper [15]. The energies and wave-functions are computed using a frozen-core configuration interaction (CI) procedure. The core $\text{Mg}^{++}(1s^2 2s^2 2p^6)$ (where electrons are assumed “frozen”) is represented by a self-consistent-field wave function. The core potential (including a dielectronic polarization term) is first used to determine Mg^+ orbitals. We then compute two-electron wave-functions by diagonalizing the 2-electron Hamiltonian in a basis of Mg^+ orbitals configurations. The multiphoton ionization rates $\Gamma_{3s^2 \rightarrow 3lk}^{(p)}$ and $\Gamma_{3lk \rightarrow k'k}^{(p)}$ are calculated within lowest order perturbation theory [16] (for the calculation of MPI matrix elements see also [17] and references therein). The rates leading to double ionization from Mg^+ are deduced from non-perturbative ATI calculations [18] (see below) and are in agreement with the perturbative results. The spatio-temporal dependence of the laser is accounted in this model by assuming the following field envelope:

$$I(r, t) = I_{max} \frac{1}{(\cosh(1.76 \frac{t}{\tau}))^2} e^{-(4 \ln 2 (\frac{r}{\kappa})^2)} \quad (2)$$

where we assume a cylindrical symmetry (r, z) for the space macro dependence of the intensity. κ and τ are respectively the spatial and temporal full width at half maximum (FWHM).

Besides the perturbative evaluations of ionization rates, we have performed non-perturbative calculations of ionization from $\text{Mg}^+(3s)$ and $\text{Mg}^+(3p)$ by numerically solving the time dependent Schrödinger equation (TDSE) [18]. A pseudo-potential [19] is used to model the Mg^+ ionic potential. The total wave-function is expanded in terms of spherical harmonics and radial B-spline functions. The total Hamiltonian is then propagated in time and the electron spectrum is calculated at the end of the pulse. This approach has the advantage of neglecting none of the couplings. It therefore accounts for all dynamical level shifts and possibly resonant transitions. These latter effects are of importance to interpret some of the experimental results as it is discussed below.

III. EXPERIMENTAL RESULTS AND COMPARISON WITH THEORY

A. Ion Yields

Figure 3 shows a typical time-of-flight ion mass spectrum obtained in the experiment, in logarithmic scale. The two charge states of magnesium (Mg^+ and Mg^{++}) are evident, each displaying peaks corresponding to its three dominant isotopes. The isotope ratios are as expected and no presence of impurities is detected. By integrating under the main peaks of such spectra obtained for different laser energies, the ion yield curves of singly and doubly ionized magnesium were obtained.

The resulting ion yield curves are shown in figure 4. The theoretical curves (given by solving equation 1 and denoted by the solid lines) agree very well with experimental values over most of the range investigated. Small discrepancies in the heavily saturated region above $2 \times 10^{13} \text{ W cm}^{-2}$ are expected since the detection volume was different to the interaction volume. The precise experimental intensity was determined by the agreement with the theoretical curves. However, some uncertainty to this estimate can be expected due to the fact that the macro-dependence of the field envelope assumed in the theory strongly

affects the ion yield behavior, especially in the saturated region, sometimes even affecting the apparent saturation intensity. The theoretical rate for three photon ionization of Mg is $\Gamma_{3s^2 \rightarrow 3sk_1}^{(3)} = 0.45 \times 10^6 \left(\frac{I}{I_0}\right)^3$ a.u. (where $I_0 = 6.44 \times 10^{15}$ W cm⁻²). The corresponding generalized cross-section $\sigma_{3s^2 \rightarrow 3sk_1}^{(3)} = 0.85 \times 10^{-80}$ cm⁶ sec² is in agreement with the values calculated by Chang and Tang [20]. One can easily calculate that single ionization saturates at about $I = 5 \times 10^{12}$ W cm² for a pulse duration of 150 fs, in agreement with the experimental ion yield shown in figure 4.

In the lower energy range of the figure (around $I = 4 \times 10^{12}$ W cm⁻²) a clear enhancement to the Mg⁺⁺ yield relative to what expected from the theoretical results can be seen. This enhancement seems to level off, the experimental curve tending back to the theoretical one, at the onset of saturation of single ionization. This may be an indication that two-electron ejection is connected to the population of the atomic ground state which would be the case for e.g. non-sequential double ionization. It should be noted that the Keldysh or adiabaticity parameter [21] $\gamma = \sqrt{I_p/(2U_p)}$ (where I_p is the ionization potential of the atom and $U_p \approx 9.33 \times 10^{-14} I(\text{W cm}^{-2})\lambda^2(\mu\text{m})$ is the ponderomotive energy of a free electron in a laser field of wavelength λ and intensity I) is not favorable to observe tunneling, rescattering or shake-off effects ($\gamma = 2$ at the highest intensity). It is therefore possible that the enhancement is related to atomic structure, or to dynamical shifts leading to either resonances or channel closing as it is discussed in section III B 1.

B. Electron results

A typical electron energy spectrum is shown in figure 5. The spectrum displays a set of main ATI peaks, each accompanied by a pronounced side peak (at approximately 1.3 eV to its low energy side). While the main ATI peak can safely be attributed to three-photon ionization of neutral magnesium leading to the ion Mg⁺(3s), the origin of the side peak is not so clear without further investigation. Note that the main peaks in figure 5 are offset compared to the expected energies corresponding to normal perturbation theory. This is an experimental artifact due to the lack of absolute energy calibration of the TOF as it is not relevant to the present investigation (see also section II A).

Table I gives the calculated energy of the ejected electrons upon ionization through the different processes depicted in figure 2. Comparing these with the electron spectra of figure 5 suggests two possible mechanisms that would result in the side peak in the recorded data: (i) 4-photon ionization of Mg leading to the Mg⁺(3p) threshold, i.e. the first excited state of the magnesium ion (process (2) in table I). That would give an energy difference between the main and side peak of $(1.656 - 0.34) = 1.316$ eV, (ii) 5-photon ionization of Mg⁺(3s) leading to the 2p⁶ ground state of Mg⁺⁺ ((4) in table I), which would give an energy difference of $(1.656 - 0.47) = 1.186$ eV. Both of these candidates are within the experimental uncertainty and the electron peak widths, especially at the higher intensities. Note that direct double ionization (process (5) in table I) would give a continuous electron distribution with maximum energy of 2.13 eV, as that energy is shared between the two electrons.

1. Electron shifts

Careful analysis of the electron spectra can give more insight into the mechanisms involved. Figure 6 shows a detail of the ATI spectra of figure 5 with additional plots for different intensities. If one concentrates just on the peak positions one notices that the main peak shifts smoothly up to a point and then stops completely. In contrast, the side peak initially shifts, then stops and finally starts shifting again. This behavior is shown clearly in figure 7 where the positions of two electron peaks are plotted versus laser intensity. The square points correspond to the main peak while the circles to the side peak.

The main peak originates from the processes (1) and (3) shown in figure 2. Our calculations show that, in all cases, the contribution from process (1) (three-photon ionization leading to a $\text{Mg}^+(3s)$ ion) dominates over (3). Indeed, this latter process originates from $\text{Mg}^+(3p)$, whose production from $\text{Mg}(3s^2)$ requires the absorption of 4 photons in contrast to the 3 photons involved in process (1). The flattening can be explained in terms of the ion production saturating [12,13]. As the intensity increases, there comes a point where, in effect, the atom will ionize before the end of the laser pulse, and so it will not experience the full power of the laser. Therefore the curve levels out. To account for the specific, detailed behavior one has to take into account all the factors that would contribute to the shift, e.g. (i) ponderomotive shifts and (ii) AC Stark shifts.

The lower data points in figure 7 (corresponding to the side peak) have a different behavior, which cannot be explained solely by saturation. The two different trends observable in the energy shift indicate that more than one process is at work. As can be seen from the theoretical calculations in figure 8(a) and (b), the side peak is a (unresolved in our data) combination of two processes, one coming from single ionization (2) the other from double sequential ionization (4) (see figure 2). At low intensity (figure 8(a)), the calculations show that the side peak is dominated by single ionization (2). At about $I = 1.8 \times 10^{13} \text{ W cm}^{-2}$, processes (2) and (4) have an equal contribution, but for higher intensities the process (4) largely dominates over (2) (figure 8(b)). Figure 8(c) and (d) indicates the development of the relevant atomic populations as the laser pulse evolves. In fact, as we will see below, the process (2) should have a significantly smaller contribution for intensities larger than $I = 8 \times 10^{12} \text{ W cm}^{-2}$. The electron production originating from the decay to the first excited ionic state would saturate at the same intensity as the electrons of the main peak, in agreement with the first trend observed in the data. On the other hand, the electrons originating from sequential double ionization (4) are expected to saturate at higher intensities. As the intensity increases, this second process dominates in the side peak, and the change of slope observed after the initial leveling off is due to the shift experienced by this second different peak. This latter shift is shown in figure 9 where we plot the energy shift of electrons originating from process (4) versus the intensity. This graph results from a non-perturbative calculation which includes both AC Stark shift and ponderomotive shift. Note that the shift is not uniquely due to the ponderomotive effect as is often the case in ATI measurements. This is shown in figure 9 where we detail the contribution of the ponderomotive shift to the total shift. It should be noted that the experimental shifts appear to have a smaller magnitude than the theoretical ones, indicating a smaller experimental intensity than previously extracted from the ion yields. However, considering that the acquisition of the electron signal takes place under different conditions to that of the ion signal (field-free, as opposed

to a high applied voltage for the ion extraction), it is extremely likely that the extraction region, and therefore the effective intensity seen by each species could well be different. The uncertainty in the determination of the intensity in the ion yields should also be taken into account, as described in a previous section.

Our calculations show that, for intensities larger than $10^{13} \text{ W cm}^{-2}$, the double ionization is dominated by the process (1+4) (see figure 2). At lower intensities, the channel (2+3) has a significant contribution to the production of Mg^{++} . As already mentioned, the double ionization yield displays a significant deviation at low intensities. We considered the laser induced energy shift of the Rydberg series $\text{Mg}(3pnl)$ (converging, as $n \rightarrow \infty$, to the sum of the AC Stark shift of $\text{Mg}^+(3p)$ and the ponderomotive shift U_p) and the AC Stark shift of $\text{Mg}(3s^2)$. Through this we found that, for intensities larger than $8 \times 10^{12} \text{ W cm}^{-2}$, the 4-photon ionization channel (2) is closed and ionization to $\text{Mg}^+(3p)$ now requires the absorption of 5 photons. The effect is that the experimental double ionization yield deviates from the normal picture at about $I = 8 \times 10^{12} \text{ W cm}^{-2}$. Note that the single ionization channel, dominated by the process (1), is almost not affected by this effect. Nevertheless, we see in figure 4 that the theoretical Mg^{++} yield lies below the experimental curve in the low intensity region. According to the previous considerations, it should fit the Mg^{++} experimental yield at low intensity and overestimate it for $I > 8 \times 10^{12} \text{ W cm}^{-2}$ (in the rate equation system (1), 4-photon ionization of Mg to $\text{Mg}^+(3p)$ is allowed at all intensities). Thus the discrepancy between theoretical and experimental results in the latter region still remains to be explained. Other effects, like direct and/or sequential ionization (eventually involving higher thresholds) enhanced by the presence of resonances, should be explored. Consequently, the sequential model adopted here for double ionization may not be valid at low intensities, where further experimental and theoretical efforts may be required in order to complete the present analysis.

IV. CONCLUSIONS

The results presented in this paper are some of the very few works studying in both experimental and theoretical detail the MPI and ATI spectra of an alkaline earth using ultra-short pulses. The work demonstrates clearly the significance of the two-electron nature of the atom in these spectra, both in terms of the role of the electron correlations, and with respect to the precise level structure of both the atom and the ion.

The attribution of the pronounced sets of side peaks, accompanying the usual ATI spectrum, was not trivial, and required a theoretical investigation taking into account all of the above factors in order to explain their origin. As it turned out, more than one processes contributed to their appearance, each dominating at a different range of intensities. Most notably, one of the two dominant processes at low intensity was the decay to the first excited electronic state of the ion, a pathway which involves the excitation of both valence electrons and coupled ionization channels. However, the prominence of this process was diminished as the intensity increased due to the depletion of the ground atomic state, and overtaken by the electron originating from sequential double ionization from the ground state of the atom. In principle, another new peak should arise due to sequential double ionization from the excited ionic state, but the position of this was calculated to be too close to the main

structure (three-photon ionization of Mg) to allow for its observation. It might be useful to conduct an extension of this study to a different photon energy, at the moment not available in our laboratory, at which these proximities are avoided, and at which the peaks from each of the processes are well resolved.

The detailed studying of the electron energy shifts of both the main and the side set of peaks also pointed to the importance of the factors mentioned above. Quite apart from their being used as a tool towards the identification of the side peak, the shifts displayed a behavior not sufficiently explained by the common analysis in terms of ponderomotive shifts. Due to the complex level structure of both the atom and the ion, with transitions close to resonance with the laser field, AC Stark shifts were found to play an important role and could no longer be ignored. The multiphoton ionization yields, despite the relatively low intensities employed, also display an interesting enhancement of double ionization which deviates from the normal picture. We have found that, due to AC and ponderomotive shifts, the channel (2) requires the absorption of 5 photons for intensities larger than $8 \times 10^{12} \text{W cm}^{-2}$. This is a possible explanation for the enhancement of double photon ionization, but other effects should be explored, in particular the possibility of near-resonant enhancement or, more tentatively, direct double ionization, possibly enhanced by electron correlations and presence of multiple doubly excited manifolds.

All of the above indicate that a full picture of the atom needs to be explicitly contained in any investigation attempting to elucidate the high-intensity behavior of two electron atoms, and possibly other atoms as well.

ACKNOWLEDGMENTS

This work has been carried out in the Ultraviolet Laser Facility of FORTH with partial support from the TMR Program of the European Union (contract number ERBFMGECT950017). We gratefully acknowledge useful discussions with Prof. P. Lambropoulos and Mr. P. Maragakis.

REFERENCES

- [1] G. Voronov and N. Delone, *JETP Lett.* **1**, 66 (1965).
- [2] P. Agostini, F. Fabre, G. Mainfray, G. Petite, and N. K. Rahman, *Phys. Rev. Lett.* **42**, 1127 (1979).
- [3] A. McPherson, G. Gibson, H. Jara, U. Johann, T. S. Luk, I. McIntyre, K. Boyer, and C. K. Rhodes, *J. Opt. Soc. Am. B* **4**, 595 (1987).
- [4] M. Ferray, A. L'Huillier, F. X. Li, L. A. Lompré, G. Mainfray, and C. Manus, *J. Phys. B* **21**, L31 (1988).
- [5] Dalwoo Kim, S. Fournier, M. Saeed, and L. F. DiMauro, *Phys. Rev. A* **41**, 4966 (1990).
- [6] L. F. DiMauro, Dalwoo Kim, M. W. Courtney, and M. Anselment, *Phys. Rev. A* **38**, 2338 (1988).
- [7] N. J. van Druten, R. Trainham, and H. G. Muller, *Phys. Rev. A* **50**, 1593 (1994).
- [8] X. Tang, T. N. Chang, P. Lambropoulos, S. Fournier, and L. F. DiMauro, *Phys. Rev. A* **41**, 5265 (1990).
- [9] Jian Zhang and P. Lambropoulos, *Phys. Rev. Lett.* **77**, 2186 (1996).
- [10] D. Strickland and G. Mourou, *Optics Commun.* **56**, 219 (1985).
- [11] Z. Bor, *Opt. Lett.* **14**, 119 (1989).
- [12] D. Charalambidis, D. Xenakis, C. J. G. J. Uiterwaal, P. Maragakis, Jian Zhang, H. Schröder, O. Faucher, and P. Lambropoulos, *J. Phys. B* **30**, 1467 (1997).
- [13] C. J. G. J. Uiterwaal, D. Xenakis, D. Charalambidis, P. Maragakis, H. Schröder, and P. Lambropoulos, *Phys. Rev. A* **57**, 392 (1998).
- [14] M. D. Perry and L. O. Landen, *Phys. Rev. A* **38**, 2815 (1988).
- [15] N. E. Karapanagioti, D. Charalambidis, C. J. G. J. Uiterwaal, C. Fotakis, H. Bachau, I. Sánchez, and E. Cormier, *Phys. Rev. A* **53**, 2587 (1996).
- [16] H. Bachau and A. Lyras, in preparation.
- [17] E. Cormier and P. Lambropoulos, *J. Phys. B* **28**, 5043 (1995).
- [18] E. Cormier and P. Lambropoulos, *J. Phys. B* **30**, 77 (1997).
- [19] P. Schwerdtfeger, H. Stoll, and H. Preuss, *J. Phys. B* **15**, 1061 (1982).
- [20] T. N. Chang and X. Tang, *Phys. Rev. A* **46**, R2209 (1992).
- [21] L. V. Keldysh, *Soviet Phys. JETP* **20**, 1307 (1965).

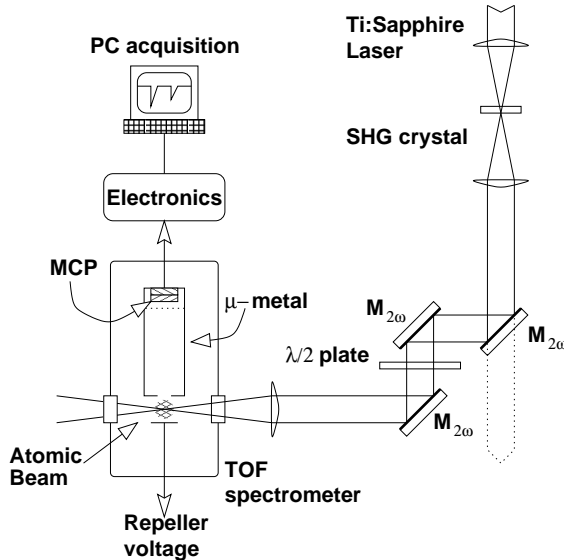


FIG. 1. Experimental setup. SHG: Second harmonic generation, $M_{2\omega}$: mirror for the second harmonic radiation, TOF: Time-of-flight, MCP: Micro-channel plates.

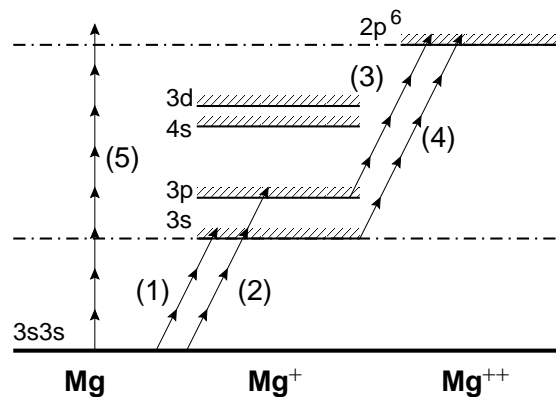


FIG. 2. Partial energy level diagram of magnesium and the relevant transitions involving 400 nm photons in the neutral atom (Mg) and its ionic states (Mg^+ and Mg^{++}). The different paths to ionization indicated by numbers (1) to (5) are described in the main text and in Table I.

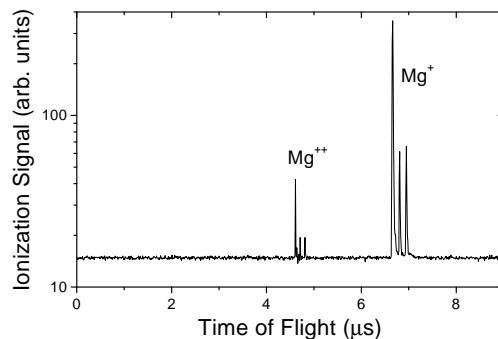


FIG. 3. Typical time of flight spectrum obtained during the experiment. While the singly and doubly ionized magnesium species can be observed, no impurities are evident. The isotopic ratios are as expected ($A=24$: 78%, 25: 10%, 26: 11%). Note the logarithmic scale.

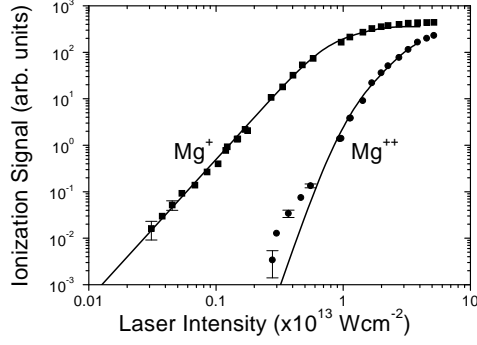


FIG. 4. Experimental and theoretical ion yields. The square data points correspond to Mg^+ whereas the circles to Mg^{++} . The solid lines are the calculated yields (rate equations and perturbation theory).

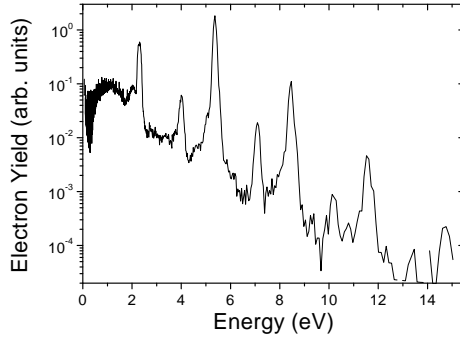


FIG. 5. Electron spectrum at a laser intensity of $2 \times 10^{13} \text{ W cm}^{-2}$. Two dominant sets of electron peaks are observable.

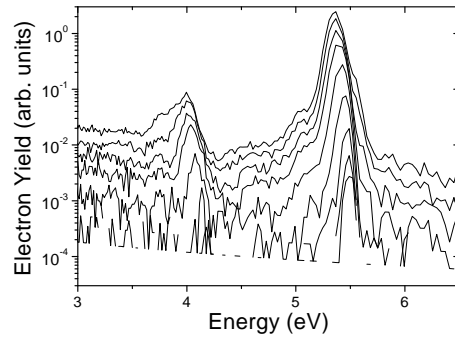


FIG. 6. Enlarged section of the electron energy spectra of figure 5 focusing on a main peak and a sub-peak, for various laser intensities. A shift of the peaks towards the higher energies as the laser power decreases is observable. (Intensities from top to bottom in $10^{13} \text{ W cm}^{-2}$: 4.7, 3.6, 2.3, 1.9, 1.4, 0.7, 0.4, 0.24, 0.22).

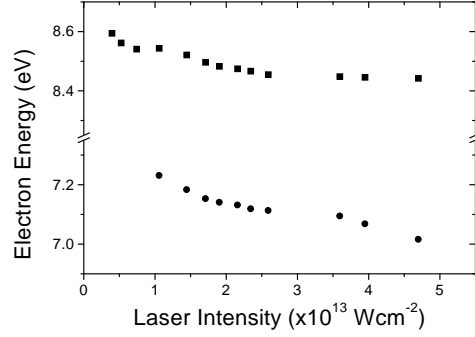


FIG. 7. Electron peak positions vs. laser intensity for a pair of peaks at approximately 8.5 eV and 7.1 eV. Note the axis break. (see text for more details).

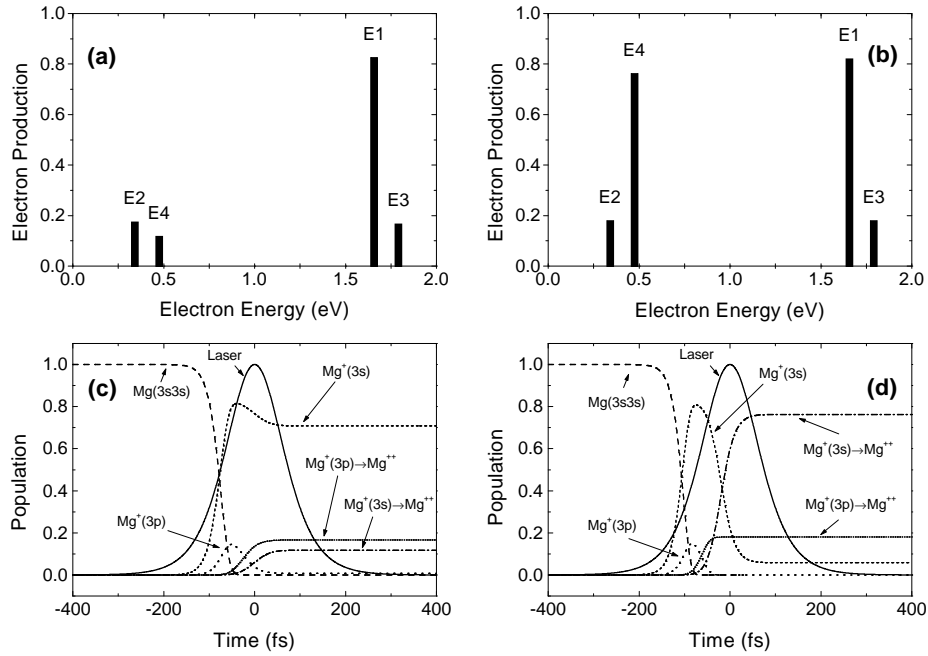


FIG. 8. Ion and electron populations calculated with no intensity space macro-dependence at two different intensities. (a), (b) Electron production at intensities of $I = 1.7 \times 10^{13} \text{ W cm}^{-2}$ and $I = 3 \times 10^{13} \text{ W cm}^{-2}$ respectively. Electron peaks correspond to processes 1-4, as indicated in figure 2; (c), (d) Time dependent populations of different ionic species at the intensities corresponding to cases (a) and (b) as the laser pulse evolves. (solid line): Laser intensity normalized to the maximum intensity; (dashed line): ground state of the atom $\text{Mg}(3s^2)$ (short-dash line): ground state of the ion $\text{Mg}^+(3s)$ produced by three-photon ionization from $\text{Mg}(3s^2)$ along with electron of energy E1; (dotted line): first excited state of the ion $\text{Mg}^+(3p)$ produced by four-photon ionization from $\text{Mg}(3s^2)$ along with electron of energy E2; (dash-dot-dot line): doubly ionized $\text{Mg}^{++}(2p^6)$ through four-photon ionization of $\text{Mg}^+(3p)$ along with electron of energy E3; (dash-dot line): doubly ionized $\text{Mg}^{++}(2p^6)$ through five-photon ionization of $\text{Mg}^+(3s)$ along with electron of energy E4;

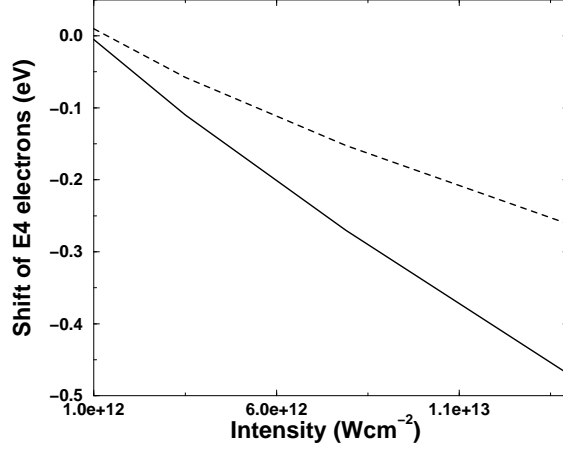


FIG. 9. Total shift (solid line) in energy of electrons originating from process (4), resulting from a non-perturbative calculation of the ionization of $\text{Mg}^+(3s)$. Also shown (dashed line) is the contribution to the total due to the $\text{Mg}^+(3s)$ AC stark shift.

TABLE I. Table of the energies of the different ionic thresholds in which the ionization may leave the Mg atoms, the number of 3.1 eV photons that need to be absorbed to reach each of these (N_{ph}) and the energy of the ejected electron upon ionization (E_{el}) (All numbers refer to field free energies, with energy shifts not taken into account). The various processes are illustrated in figure 2.

No	Transition	Energy (eV)	N_{ph}	E_{el} (eV)
(1)	$\text{Mg}(3s^2) \rightarrow \text{Mg}^+(3s)$	7.644	3	1.656
(2)	$\text{Mg}(3s^2) \rightarrow \text{Mg}^+(3p)$	12.06	4	0.34
(3)	$\text{Mg}^+(3p) \rightarrow \text{Mg}^{++}(2p^6)$	10.614	4	1.786
(4)	$\text{Mg}^+(3s) \rightarrow \text{Mg}^{++}(2p^6)$	15.03	5	0.47
(5)	$\text{Mg}(3s^2) \rightarrow \text{Mg}^{++}(2p^6)$	22.674	8	2.13